

Beam spin asymmetry in deep and exclusive π^0 electroproduction

R. De Masi,^{1,30} M. Garçon,¹ B. Zhao,² M.J. Amarian,²⁹ P. Ambrozewicz,¹² M. Anghinolfi,¹⁸ G. Asryan,⁴⁰ H. Avakian,³⁵ H. Bagdasaryan,²⁹ N. Baillie,³⁹ J. Ball,¹ J.P. Ball,⁴ N.A. Baltzell,³⁴ V. Batourine,²³ M. Battaglieri,¹⁸ I. Bedlinskiy,¹⁹ M. Bellis,⁷ N. Benmouna,¹⁴ B.L. Berman,¹⁴ P. Bertin,^{35,20} A.S. Biselli,^{7,11} L. Blaszczyk,¹³ S. Bouchigny,³⁰ S. Boiarinov,³⁵ R. Bradford,⁷ D. Branford,¹⁰ W.J. Briscoe,¹⁴ W.K. Brooks,³⁵ S. Bültmann,²⁹ V.D. Burkert,³⁵ C. Butuceanu,³⁹ J.R. Calarco,²⁶ S.L. Careccia,²⁹ D.S. Carman,³⁵ L. Casey,⁸ S. Chen,¹³ L. Cheng,⁸ P.L. Cole,¹⁶ P. Collins,⁴ P. Coltharp,¹³ D. Crabb,³⁸ V. Crede,¹³ N. Dashyan,⁴⁰ E. De Sanctis,¹⁷ R. De Vita,¹⁸ P.V. Degtyarenko,³⁵ A. Deur,³⁵ K.V. Dharmawardane,²⁹ R. Dickson,⁷ C. Djalali,³⁴ G.E. Dodge,²⁹ J. Donnelly,¹⁵ D. Doughty,^{9,35} M. Dugger,⁴ O.P. Dzyubak,³⁴ H. Egiyan,³⁵ K.S. Egiyan,⁴⁰ L. El Fassi,³ L. Elouadrhiri,³⁵ P. Eugenio,¹³ G. Fedotov,²⁵ G. Feldman,¹⁴ A. Fradi,³⁰ H. Funsten,³⁹ G. Gavalian,²⁹ G.P. Gilfoyle,³³ K.L. Giovanetti,²² F.X. Girod,^{1,35} J.T. Goetz,⁵ A. Gonenc,¹² R.W. Gothe,³⁴ K.A. Griffioen,³⁹ M. Guidal,³⁰ N. Guler,²⁹ L. Guo,³⁵ V. Gyurjyan,³⁵ K. Hafidi,³ H. Hakobyan,⁴⁰ C. Hanretty,¹³ F.W. Hersman,²⁶ K. Hicks,²⁸ I. Hleiqawi,²⁸ M. Holtrop,²⁶ C.E. Hyde-Wright,²⁹ Y. Ilieva,¹⁴ D.G. Ireland,¹⁵ B.S. Ishkhanov,²⁵ E.L. Isupov,²⁵ M.M. Ito,³⁵ D. Jenkins,³⁷ H.S. Jo,³⁰ J.R. Johnstone,¹⁵ K. Joo,² H.G. Juengst,^{14,29} N. Kalantarians,²⁹ J.D. Kellie,¹⁵ M. Khandaker,²⁷ W. Kim,²³ A. Klein,²⁹ F.J. Klein,⁸ A.V. Klimenko,²⁹ M. Kossov,¹⁹ Z. Krahn,⁷ L.H. Kramer,^{12,35} V. Kubarovskiy,^{31,35} J. Kuhn,⁷ S.E. Kuhn,²⁹ S.V. Kuleshov,¹⁹ J. Lachniet,^{7,29} J.M. Laget,³⁵ J. Langheinrich,³⁴ D. Lawrence,²⁴ T. Lee,²⁶ K. Livingston,¹⁵ H.Y. Lu,³⁴ M. MacCormick,³⁰ N. Markov,² P. Mattione,³² M. Mazouz,²¹ B. McKinnon,¹⁵ B.A. Mecking,³⁵ M.D. Mestayer,³⁵ C.A. Meyer,⁷ T. Mibe,²⁸ B. Michel,²⁰ K. Mikhailov,¹⁹ M. Mirazita,¹⁷ R. Miskimen,²⁴ V. Mokeev,^{25,35} B. Moreno,³⁰ K. Moriya,⁷ S.A. Morrow,^{1,30} M. Moteabbed,¹² E. Munevar,¹⁴ G.S. Mutchler,³² P. Nadel-Turonski,¹⁴ R. Nasseripour,^{12,34} S. Niccolai,³⁰ G. Niculescu,²² I. Niculescu,²² B.B. Niczyporuk,³⁵ M.R. Niroula,²⁹ R.A. Niyazov,³⁵ M. Nozar,³⁵ M. Osipenko,^{18,25} A.I. Ostrovidov,¹³ K. Park,²³ E. Pasyuk,⁴ C. Paterson,¹⁵ S. Anefalos Pereira,¹⁷ J. Pierce,³⁸ N. Pivnyuk,¹⁹ D. Pocanic,³⁸ O. Pogorelko,¹⁹ S. Pozdniakov,¹⁹ J.W. Price,⁶ S. Procureur,¹ Y. Prok,^{38,35} D. Protopopescu,¹⁵ B.A. Raue,^{12,35} G. Ricco,¹⁸ M. Ripani,¹⁸ B.G. Ritchie,⁴ F. Ronchetti,¹⁷ G. Rosner,¹⁵ P. Rossi,¹⁷ F. Sabatié,¹ J. Salamanca,¹⁶ C. Salgado,²⁷ J.P. Santoro,⁸ V. Sapunenko,³⁵ R.A. Schumacher,⁷ V.S. Serov,¹⁹ Y.G. Sharabian,³⁵ D. Sharov,²⁵ N.V. Shvedunov,²⁵ E.S. Smith,³⁵ L.C. Smith,³⁸ D.I. Sober,⁸ D. Sokhan,¹⁰ A. Stavinsky,¹⁹ S. Stepanyan,³⁵ S.S. Stepanyan,²³ B.E. Stokes,¹³ P. Stoler,³¹ I.I. Strakovsky,¹⁴ S. Strauch,^{14,34} M. Taiuti,¹⁸ D.J. Tedeschi,³⁴ A. Tkabladze,^{28,14} S. Tkachenko,²⁹ C. Tur,³⁴ M. Ungaro,² M.F. Vineyard,³⁶ A.V. Vlassov,¹⁹ E. Voutier,²¹ D.P. Watts,¹⁵ L.B. Weinstein,²⁹ D.P. Weygand,³⁵ M. Williams,⁷ E. Wolin,³⁵ M.H. Wood,³⁴ A. Yegneswaran,³⁵ L. Zana,²⁶ J. Zhang,²⁹ and Z.W. Zhao³⁴

(The CLAS Collaboration)

¹CEA-Saclay, Service de Physique Nucléaire, 91191 Gif-sur-Yvette, France

²University of Connecticut, Storrs, Connecticut 06269

³Argonne National Laboratory, Argonne, Illinois 60439

⁴Arizona State University, Tempe, Arizona 85287-1504

⁵University of California at Los Angeles, Los Angeles, California 90095-1547

⁶California State University, Dominguez Hills, Carson, CA 90747

⁷Carnegie Mellon University, Pittsburgh, Pennsylvania 15213

⁸Catholic University of America, Washington, D.C. 20064

⁹Christopher Newport University, Newport News, Virginia 23606

¹⁰Edinburgh University, Edinburgh EH9 3JZ, United Kingdom

¹¹Fairfield University, Fairfield CT 06824

¹²Florida International University, Miami, Florida 33199

¹³Florida State University, Tallahassee, Florida 32306

¹⁴The George Washington University, Washington, DC 20052

¹⁵University of Glasgow, Glasgow G12 8QQ, United Kingdom

¹⁶Idaho State University, Pocatello, Idaho 83209

¹⁷INFN, Laboratori Nazionali di Frascati, 00044 Frascati, Italy

¹⁸INFN, Sezione di Genova, 16146 Genova, Italy

¹⁹Institute of Theoretical and Experimental Physics, Moscow, 117259, Russia

²⁰LPC Clermont-Ferrand, Université Blaise Pascal, CNRS/IN2P3, 63177 Aubière, France

²¹LPSC, Université Joseph Fourier, CNRS/IN2P3, INPG, 38026 Grenoble, France

²²James Madison University, Harrisonburg, Virginia 22807

²³Kyungpook National University, Daegu 702-701, South Korea

²⁴University of Massachusetts, Amherst, Massachusetts 01003

²⁵Moscow State University, General Nuclear Physics Institute, 119899 Moscow, Russia

²⁶University of New Hampshire, Durham, New Hampshire 03824-3568

²⁷Norfolk State University, Norfolk, Virginia 23504

²⁸Ohio University, Athens, Ohio 45701

²⁹Old Dominion University, Norfolk, Virginia 23529

³⁰Institut de Physique Nucléaire, 91406 Orsay, France

³¹Rensselaer Polytechnic Institute, Troy, New York 12180-3590

³²Rice University, Houston, Texas 77005-1892

³³University of Richmond, Richmond, Virginia 23173

³⁴University of South Carolina, Columbia, South Carolina 29208

³⁵Thomas Jefferson National Accelerator Facility, Newport News, Virginia 23606

³⁶Union College, Schenectady, NY 12308

³⁷Virginia Polytechnic Institute and State University, Blacksburg, Virginia 24061-0435

³⁸University of Virginia, Charlottesville, Virginia 22901

³⁹College of William and Mary, Williamsburg, Virginia 23187-8795

⁴⁰Yerevan Physics Institute, 375036 Yerevan, Armenia

(Dated: October 29, 2018)

The beam spin asymmetry (BSA) in the exclusive reaction $\bar{e}p \rightarrow ep\pi^0$ was measured with the CEBAF 5.77 GeV polarized electron beam and Large Acceptance Spectrometer (CLAS). The x_B , Q^2 , t and ϕ dependences of the π^0 BSA are presented in the deep inelastic regime. The asymmetries are fitted with a $\sin\phi$ function and their amplitudes are extracted. Overall, they are of the order of 0.04 - 0.11 and roughly independent of t . This is the signature of a non-zero longitudinal-transverse interference. The implications concerning the applicability of a formalism based on generalized parton distributions, as well as the extension of a Regge formalism at high photon virtualities, are discussed.

PACS numbers: 12.40.Vv,13.40.Gp,13.60.Hb,13.60.Le,13.60.-r,14.20.Dh,24.85.+p

I. INTRODUCTION

Deeply virtual exclusive reactions $\gamma^*N \rightarrow N\gamma, N\pi, N\rho, \dots$, where the γ^* virtuality Q^2 is large, have the potential to probe nucleon structure at the parton level, as described by generalized parton distributions (GPDs). These distributions are universal functions which parameterize the non-perturbative structure of the nucleon. They include as limiting cases form factors and parton distributions, and they also provide access to hitherto unknown observables like the spatial distribution of partons of given longitudinal momentum fraction or the angular momentum of quarks and gluons inside the nucleon [1, 2, 3]. The description of deeply virtual meson production in terms of GPDs relies on a factorization theorem [4], which applies when the virtual photon γ^* is longitudinally polarized. In other words, meson production is expected to proceed mostly through longitudinal virtual photons in the Bjorken regime ($Q^2 \rightarrow \infty$ and the Bjorken variable x_B finite). The corresponding leading-twist diagram (or handbag diagram, illustrated in Fig. 1) for π^0 production is sensitive to specific flavour combinations of quark-helicity dependent (or ‘‘polarized’’) GPDs: $\frac{2}{3}\tilde{H}^u + \frac{1}{3}\tilde{H}^d$ and $\frac{2}{3}\tilde{E}^u + \frac{1}{3}\tilde{E}^d$ [3]. The \tilde{H}^q are partly constrained by the polarized parton distributions Δq , while the \tilde{E}^q , largely unknown, are often modeled by a pion-pole term, which would not contribute to the $ep \rightarrow ep\pi^0$ process [3]. The Q^2 range in which the handbag diagram dominates, or where its contribution can be safely extracted, is not yet known for meson production.

An alternative description of exclusive meson produc-

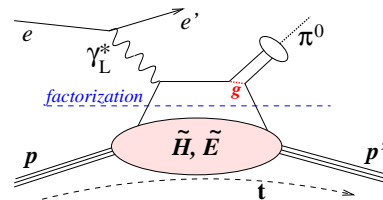


FIG. 1: (Color online) Schematic representation of the handbag diagram for neutral pion production. The symbol g stands for a gluon exchange between quark lines.

tion is based on Regge models, where trajectories are exchanged in the t -channel as mediators of the interaction. While extensively studied for photoproduction [5], i.e. for $Q^2 = 0$ and transverse photons, the extension and applicability to virtual photons has not yet been considered in the specific case of neutral pion production.

So, two theoretical descriptions are *a priori* possible. The Regge approach starts from $Q^2 = 0$ and must be extended to non-zero Q^2 , while the GPD approach has a firm QCD foundation in the Bjorken regime, and its applicability must be tested at finite values of Q^2 .

On the experimental side, while the focus has recently been on the production of real photons [6] (the so-called deeply virtual Compton scattering process, or DVCS) and of vector mesons [7, 8, 9], there is essentially no experimental data available on neutral pseudoscalar meson production above the resonance region. Cross sections were measured at DESY [10] at low values of Q^2 , while a first result on the target-spin asymmetry was obtained at CLAS [11]. For recent data on charged pion electro-

production in this kinematic regime, see Refs. [12, 13].

The $ep \rightarrow ep\pi^0$ observables depend on the Q^2 and x_B variables, on the squared four-momentum transfer t to the proton and on the angle ϕ between the leptonic and hadronic planes. The polarization of the exchanged virtual photon may be transverse (T) or longitudinal (L). It induces an azimuthal dependence of the reduced cross section for the $\gamma^*p \rightarrow p\pi^0$ process. For each (x_B, Q^2, t) , taking the ratio of the difference over the sum of cross sections for opposite beam helicities, the beam spin asymmetry (BSA) has the following ϕ dependence:

$$A = \frac{\overrightarrow{\sigma} - \overleftarrow{\sigma}}{\overrightarrow{\sigma} + \overleftarrow{\sigma}} = \frac{\alpha \sin \phi}{1 + \beta \cos \phi + \gamma \cos 2\phi}. \quad (1)$$

The parameter α is proportional to a term denoted $\sigma_{LT'}$, originating from the imaginary part of an interference between the helicity amplitudes describing the process [14].

$$\alpha = \frac{\sqrt{2\epsilon(1-\epsilon)}\sigma_{LT'}}{\sigma_T + \epsilon\sigma_L}, \quad (2)$$

where σ_T and σ_L are the pure transverse and longitudinal cross sections, and ϵ is the usual virtual photon polarization parameter. Any measurement of a non-zero BSA would be indicative of an L - T interference, and therefore of contributions that cannot be described in terms of GPDs. Indeed, preliminary CLAS data indicated sizeable BSA both for exclusive π^+ and π^0 production at large Q^2 [15].

II. EXPERIMENT AND DATA ANALYSIS

This experiment used the CEBAF 5.77 GeV longitudinally-polarized electron beam impinging on a 2.5-cm long liquid-hydrogen target. The beam helicity was switched pseudo-randomly at a frequency of 30 Hz, and the beam polarization, measured with a Møller polarimeter, had an average value of 79.4%. All final-state particles from the reaction $ep \rightarrow ep\pi^0$ followed by the decay $\pi^0 \rightarrow \gamma\gamma$ were detected. The six-sector CLAS spectrometer [16] was used in order to detect scattered electrons, recoil protons and photons emitted at large angles. An additional small electromagnetic calorimeter ensured photon detection in the near forward region ($4.5 - 15^\circ$). This inner calorimeter (IC) was built of 424 tapered lead-tungstate crystals, read out with avalanche photodiodes. It was calibrated using the two-photon decay of (inclusively produced) neutral pions.

Events were selected if an electron had generated a trigger, one and only one proton was identified and any number of photons (above an energy threshold of 150 MeV) were detected in either the IC or the standard CLAS calorimeter EC [17]. Electrons were identified through signals in the EC and in the Čerenkov counters. Events considered hereafter included the kinematic requirements : $Q^2 > 1 \text{ GeV}^2$, γ^*p invariant mass $W > 2 \text{ GeV}$ and scattered electron energy $E' > 0.8 \text{ GeV}$.

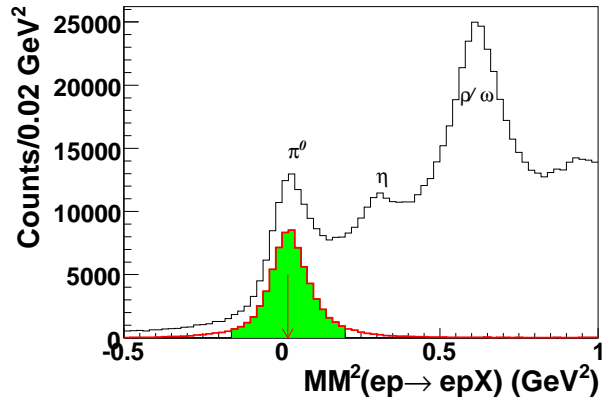


FIG. 2: (Color online) Distribution of squared missing mass for the $ep \rightarrow epX$ reaction before (black line) and after (thick red line) all cuts on other variables are applied. The arrow points to the pion mass, while the shaded green area correspond to the selected events.

Protons were unambiguously identified over the whole momentum range of interest using time-of-flight from the target to the CLAS scintillators, as well as the track length and momentum determined by the drift chambers. A cut at $\pm 3\sigma$ was applied around the pion mass in the squared missing mass $MM^2(ep \rightarrow epX)$ distribution to exclude multipion background.

All clusters detected in the IC were assumed to originate from photons, while additional time-of-flight information was used in the EC to separate photons from neutrons. Photons hitting the calorimeters' edges were excluded. In addition, since the most forward hits in the IC had a sizeable probability of originating from Møller accidental coincidences, a minimal angle was imposed on all photon candidates: $\theta_\gamma > 8^\circ - 0.75^\circ \times (E_\gamma/1 \text{ GeV})$.

In order to reconstruct the π^0 candidates, the two most energetic detected photons were considered, originating from either calorimeter. Four combinations are then possible: IC-IC, IC-EC, EC-IC, EC-EC, where the photon with the highest energy was in the first mentioned calorimeter. The two calorimeters (IC and EC) had similar angular resolutions (about 4 mrad for 1 GeV photons) but different energy resolutions ($\sigma_{E_\gamma}/E_\gamma \simeq 4.5\%$ for IC and 11.6% for EC). When considering photon pairs, the kinematic cuts described below depended then on the four possible photon configurations defined previously.

Events were then selected using a cut at $\pm 3\sigma$ in the squared missing mass $MM^2(ep \rightarrow e\pi^0 X)$ and a cut in the cone angle between the expected direction of the pion from $ep \rightarrow epX$ kinematics and the measured direction of the two-photon system. This selection resulted in very clean peaks in all kinematic correlations (Fig. 2 gives one example) and in the distributions of the two-photon invariant mass (see Fig. 3), with respectively 191k, 12k, 7k and 14k events. The small remaining background was estimated using side-bands on the two-photon invariant

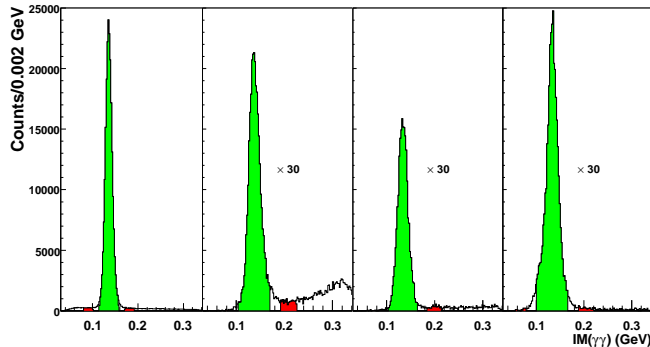


FIG. 3: (Color online) Distributions of the two-photon invariant mass, after the application of all cuts described in the text, for the four configurations IC-IC, IC-EC, EC-IC, EC-EC, from left to right. The shaded areas correspond to the selected peaks (in green) and to the side-bands used in the background subtraction (in red). Note the change of scale for the last three configurations.

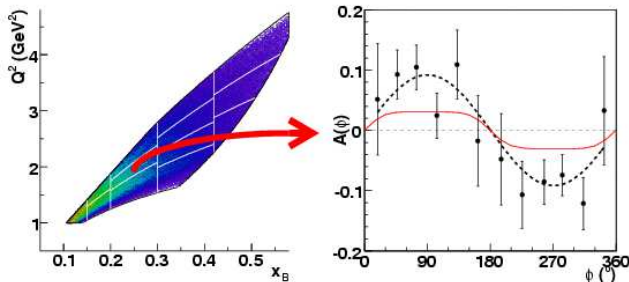


FIG. 4: (Color online) Left: kinematic coverage and binning in the (x_B, Q^2) plane. Right: $A(\phi)$ for one of the 13 (x_B, Q^2) bins and one of the 5 bins in t , corresponding to $\langle x_B \rangle = 0.249$, $\langle Q^2 \rangle = 1.95 \text{ GeV}^2$ and $\langle t \rangle = -0.29 \text{ GeV}^2$; the black dashed curve corresponds to a fit with $A \simeq \alpha \sin \phi$ and the red solid curve to the JML model discussed in the text.

mass spectra, for each beam helicity state and for each of the elementary bins in $(x_B, Q^2, t$ and $\phi)$.

III. π^0 ASYMMETRY

The data were divided into thirteen bins in the (x_B, Q^2) plane (see Fig. 4), five bins in $-t$ (defined by the bin limits 0.09, 0.2, 0.4, 0.6, 1 and 1.8 GeV^2) and twelve 30° bins in ϕ . The resolutions in all corresponding variables are smaller than the bin sizes. Bin centering corrections were applied.

Within statistical accuracy, the ϕ -distributions were found to be compatible with $A \simeq \alpha \sin \phi$ in each t -bin (Fig. 4 right). The same compatibility was observed when the ϕ -distributions were integrated in t . The determination of the asymmetry amplitude at 90° was stable whether the terms in $\cos \phi$ and $\cos 2\phi$ in Eq. (1) were included in the fit or not. Figure 5 gives the values

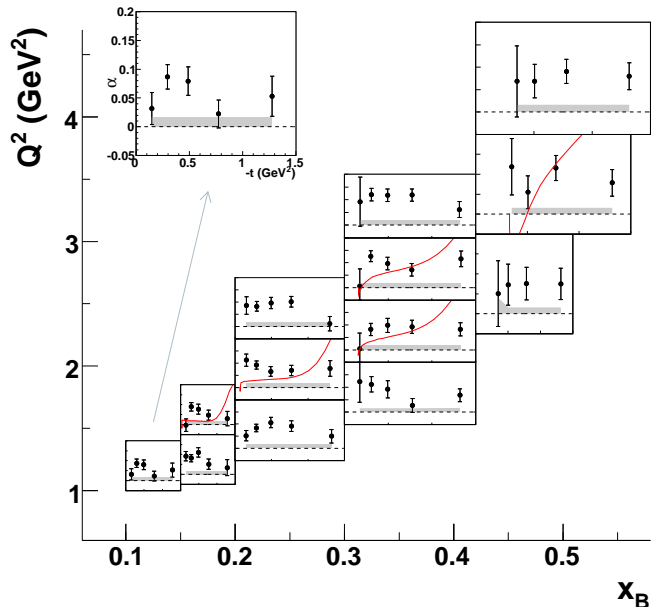


FIG. 5: (Color online) Fit parameter α , as extracted from $A \simeq \alpha \sin \phi$, as a function of $-t$. The location of each individual plot corresponds to the approximate coverage in (x_B, Q^2) , except the upper left one (an enlargement of the lower left one) which indicates the scales common to all plots. The grey areas indicate the maximal size of systematic uncertainties. For selected kinematics, the red curves correspond to the JML model discussed in the text.

of α in the 62 (x_B, Q^2, t) bins considered. By conservation of angular momentum, the helicity-flip transverse amplitude, and thus A and α , are identically zero as t reaches its kinematic limit t_0 , corresponding to π^0 s emitted in the direction of the virtual photon. At small x_B , the value of $-t_0$ is smaller than our first bin limit 0.09 GeV^2 (corresponding to the proton-energy detection threshold), which is why A does not go to zero. The increase of $-t_0$ explains the missing t -bins at large x_B .

Systematic uncertainties arise from the event selection, as well as from the choice of the fit function used to extract α . Together, they were estimated at 0.016. The comparison between two separate analyses led to increase this value for two points in Fig. 5. The beam polarization measurements induce an additional overall relative uncertainty of 3.5%. The data set may be found in [18]

IV. DISCUSSION OF THE RESULTS

As seen in Fig. 5, the measured beam spin asymmetries are systematically of the order of 0.04 to 0.11, over a wide kinematic range in x_B, Q^2 and t . In particular, there is no evidence of a decrease of $\alpha(t)$ as a function of Q^2 . This is a clear sign of a non-zero LT' interference among the amplitudes describing the $\gamma^* p \rightarrow p\pi^0$ reaction.

In the GPD formalism, only the longitudinal ampli-

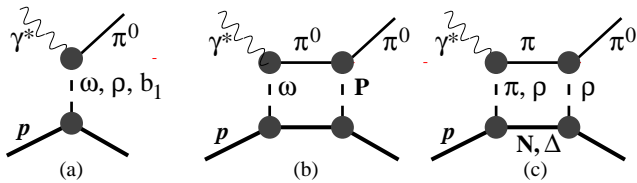


FIG. 6: Diagrams describing the neutral pion production in the JML model: (a) Pole terms. (b) Box diagram with elastic π^0 rescattering. (c) Box diagram with charge exchange ($\pi^+N, \pi^+\Delta^0, \pi^-\Delta^{++}$ are the three intermediate states considered). The exchanged mesons are to be understood as the corresponding Regge trajectories, and \mathbf{P} stands for the Pomeron.

tude, dominant in the Bjorken regime, is calculated. The present evidence of non-zero transverse terms indicates that it may be necessary to perform a L/T separation in order to isolate the longitudinal part of the cross section.

A Regge-type model (JML) describes the pion photo- and electroproduction according to the diagrams in Fig. 6. The model parameters are tuned to describe the photoproduction data. In particular the strength of the b_1 exchange term is adjusted to reproduce the linearly polarized photon beam asymmetry [5]. In extending the model to the case of electroproduction, vertex electromagnetic form factors are adjusted to reproduce the DESY data [10]. The application to the kinematic range of the present data is then an extrapolation of the model, which will be fully described elsewhere [19] and reproduces the target-spin asymmetry [11]. When considering the pole terms, only the b_1 exchange, through its interference with the ρ and ω exchanges (because of opposite parities), may generate a non-zero beam spin asymmetry. Treating the box diagrams in the approximation of on-shell intermediate particles yields the solid curves presented in Figs. 4 and 5. As apparent in Fig. 4, the model generates sizeable γ and β terms in Eq. (1), corresponding respectively to a TT interference due to the pole terms of Fig. 6a and to a LT interference due to the box diagrams of Fig. 6c.

V. SUMMARY

Sizeable beam-spin asymmetries for exclusive neutral pion electroproduction off the proton have been measured above the resonance region for the first time. These non-zero asymmetries imply that both transverse and longitudinal amplitudes participate in the process. The determination of the longitudinal cross section in the kinematic regime considered here, and the subsequent extraction of polarized generalized parton distributions, may then necessitate to perform a L/T separation. For the same purpose, measurements at still higher values of Q^2 would be crucial in providing evidence for the expected decrease of the transverse cross section. Presently, the only available model to calculate this observable is based on Regge theory. It reproduces the magnitude of the asymmetries at intermediate values of t , but does not exhibit the measured kinematic dependences. Beam-spin asymmetries for exclusive η electroproduction, as well as cross sections for π^0 and η meson production, will be considered in forthcoming publications.

Acknowledgments

We acknowledge the outstanding efforts of the staff of the Accelerator and Physics Divisions at JLab, as well as of the technical staff at DAPNIA-Saclay and IPN-Orsay, that made this experiment possible. This work was supported in part by the French Centre National de la Recherche Scientifique and Commissariat à l’Energie Atomique, the U.S. Department of Energy and National Science Foundation, the Italian Istituto Nazionale di Fisica Nucleare, the Korean Science and Engineering Foundation, the U.K. Engineering and Physical Science Research Council. The Jefferson Science Associates (JSA) operates the Thomas Jefferson National Accelerator Facility for the United States Department of Energy under contract DE-AC05-06OR23177.

-
- [1] X.-D. Ji, Phys. Rev. Lett. **78**, 610 (1997).
 - [2] M. Burkardt, Phys. Rev. D **62**, 071503 (2000).
 - [3] M. Diehl, Phys. Rep. **388**, 41 (2003).
 - [4] J. C. Collins, L. Frankfurt, and M. Strikman, Phys. Rev. D **56**, 2982 (1997).
 - [5] M. Guidal, J. Laget, and M. Vanderhaeghen, Nucl. Phys. **A627**, 645 (1997).
 - [6] M. Garçon, AIP Conf. Proc. **870**, 93 (2006).
 - [7] A. Airapetian et al. (HERMES), Eur. Phys. J. C **17**, 389 (2000).
 - [8] C. Hadjidakis et al. (CLAS), Phys. Lett. **B605**, 256 (2005).
 - [9] L. Morand et al. (CLAS), Eur. Phys. J. A **24**, 445 (2005).
 - [10] F. Brasse et al., Phys. Lett. **B58**, 467 (1975).
 - [11] S. Chen et al. (CLAS), Phys. Rev. Lett. **97**, 072002 (2006).
 - [12] A. Airapetian et al. (HERMES) (2007), submitted to Phys. Lett. B, arXiv:0707.0222 [hep-ex].
 - [13] T. Horn et al. (2007), arXiv:0707.1794 [nucl-ex].
 - [14] D. Drechsel and L. Tiator, J. Phys. G **18**, 449 (1992).
 - [15] H. Avakian and L. Elouadrhiri, Proc. High Energy Spin Physics, A.V. Efremov and O.V. Teryaev Editors, Dubna (2003).
 - [16] B. A. Mecking et al. (CLAS), Nucl. Instr. Meth. **A503**, 513 (2003).
 - [17] M. Amarian et al., Nucl. Instr. Meth. **A460**, 239 (2001).
 - [18] CLAS Physics Data Base, URL <http://clasweb.jlab.org/physicsdb/cover.html>.
 - [19] J. M. Laget, in preparation.